Nutrition 62 (2019) 63–73

Contents lists available at ScienceDirect

Nutrition

journal homepage: www.nutritionjrnl.com

Basic nutritional investigation

Lactobacillus brevis DM9218 ameliorates fructose-induced hyperuricemia through inosine degradation and manipulation of intestinal dysbiosis

Haina Wang Ph.D. [a,b], Lu Mei Ph.D. [c], Ying Deng M.S. [d], Yinhui Liu Ph.D. [d], Xiaoqing Wei M.S. [d], Man Liu M.S. [d], Jiaorui Zhou M.S. [d], Hong Ma M.S. [d], Pengyuan Zheng Ph.D. [c], Jieli Yuan M.S. [d], Ming Li Ph.D. [d,*]

[a] *Department of Hematology, Liaoning Key Laboratory of Hematopoietic Stem Cell Transplantation and Translational Medicine, Second Hospital of Dalian Medical University, Dalian, China*
[b] *Center for molecular medicine, School of Life Science and Biotechnology, Dalian University of Technology, Dalian, China*
[c] *Department of Gastroenterology, the Fifth Affiliated Hospital of Zhengzhou University, Zhengzhou, China*
[d] *College of Basic Medical Sciences, Dalian Medical University, Dalian, China*

ARTICLE INFO

Article History:
Received 24 July 2018
Received in revised form 2 October 2018
Accepted 17 November 2018

Keywords:
Lactobacillus
Fructose
Hyperuricemia
Inosine
Intestinal dysbiosis
Xanthine oxidase

ABSTRACT

Objective: High fructose consumption exacerbates purine degradation and intestinal dysbiosis, which are closely related to the development of hyperuricemia. Probiotics are powerful weapons to combat metabolic disturbance and intestinal dysbiosis. Previously we isolated a *Lactobacillus* strain named DM9218 that could reduce the serum uric acid (UA) level by assimilating purine nucleosides. The present study aimed to evaluate the effects of DM9218 on high-fructose–induced hyperuricemia and to elucidate the underlying mechanisms.
Methods: Mice were fed a normal diet, a high-fructose diet, or high-fructose diet with DM9218. Metabolic parameters, fructose- and UA-related metabolites, and fecal microbiota were investigated. Whole-genome sequencing of strain DM9218 was also conducted. In addition, an inosine hydrolase from DM9218 was heterologously expressed in *Escherichia coli*, and its inosine-degrading activity was detected.
Results: Our results indicated that DM9218 could decrease serum UA level and hepatic xanthine oxidase activity in fructose-fed mice. It could protect against high-fructose–induced liver damage and retard UA accumulation by degrading inosine. The modulation effect of DM9218 on high-fructose–induced intestinal dysbiosis resulted in enhancement of intestinal barrier function and reduction of liver lipopolysaccharide, which was closely correlated with the down-regulation of inflammatory cytokine–stimulated xanthine oxidase expression and activity.
Conclusions: Lactobacillus brevis DM9218 is a probiotic strain with the potential to ameliorate fructose-induced hyperuricemia.

Introduction

Fructose consumption in the form of high-fructose corn syrup in soft drinks and processed foods has increased dramatically in recent years. Absorption of fructose is aided by glucose transporters, and it is metabolized in the liver [1]. Triglyceride (TG), free fatty acid, uric acid (UA), and methylglyoxal are fructose degradation products; high levels of these products are dangerous to the body. Moreover, adenosine triphosphate (ATP) depletion and reactive oxygen species production during fructose metabolism stimulate overproduction of inflammatory cytokines and endotoxins, which are also risk factors for health [2]. Emerging evidence suggests that increased dietary consumption of fructose can elevate the risk of development of diseases and disorders including metabolic syndrome, chronic renal disease, insulin resistance [3], cardiovascular disease [4], and type 2 diabetes [5,6].

High fructose intake is in particular a risk factor for hyperuricemia (excess uric acid in the blood). Metabolism of fructose can activate adenosine monophosphate (AMP) deaminase and enhance purine degradation and the production of inosine, which results in elevation of serum uric acid [7]. In addition, long-term fructose

This study was supported by the Nature Science Foundation of Liaoning Province, China (2015020262), the China Postdoctoral Science Foundation (2016M601317, 2018T110225), and the Research Foundation from the Department of Education, Liaoning Province, China (L2016003). This work was also supported by Liaoning Provincial Program for Top Discipline of Basic Medical Sciences.
* Corresponding author. Tel.: +86-411-86110305.
E-mail address: vivianmarat@163.com (M. Li).

https://doi.org/10.1016/j.nut.2018.11.018
0899-9007/

consumption can suppress ileal uric acid excretion through activation of nicotinamide adenine dinucleotide phosphate oxidase, leading to a further increase of the uric acid level [8]. Hyperuricemia is well known as a cause of gout. In recent years a number of epidemiologic studies have also found a correlation between hyperuricemia and the development of hypertension, obesity, renal disease [9], cardiovascular disease [10], and diabetes [11]. Studies in animal models suggested that cardiovascular and kidney diseases could benefit from lowering serum uric acid [12–14].

Although much attention has been paid to pharmacologic interventions to reduce serum uric acid [15,16], diet has long been identified as a non-negligible determinant of serum uric acid level [17,18]. To reduce serum uric acid levels, patients are usually told to limit their consumption of certain purine-rich foods like organ meats and shellfish. The intestinal microbiota must also be considered another important determinant of serum uric acid level because they directly take part in food digestion and absorption [19]. Intestinal dysbiosis was found in patients with gout [20], which highlighted its role in purine degradation and regulation of uric acid accumulation. Therefore manipulation of intestinal dysbiosis may contribute to the prevention of hyperuricemia.

Probiotics are powerful weapons to combat intestinal dysbiosis [21]. In the past few years, probiotics have rapidly emerged as potential natural therapeutics for metabolic syndrome [22]. Probiotic microorganisms are well known for their beneficial effect in modulating intestinal microbiota and their contribution to health and well-being [23,24]. However, to our knowledge, few studies have considered the beneficial effects of probiotics on high-fructose–induced hyperuricemia. Previously we isolated a *Lactobacillus* strain named DM9218 from Chinese sauerkraut; this strain could efficiently reduce serum uric acid levels by assimilating purine nucleosides (inosine and guanosine) and exhibited good potential in hyperuricemia prevention [25]. The present study aimed to evaluate the effects of DM9218 on high-fructose–induced hyperuricemia in a mouse model and to investigate the underlying mechanisms.

Methods

Animals

BALB/c male mice raised under specific pathogen-free conditions were assigned to three groups ($n = 15$ in each group): a control group fed with standard diet and normal drinking water; a high-fructose group (HF group) with standard diet and 15% fructose solution; and a probiotic-treated group (probiotic group) with standard diet, 15% fructose solution, and DM9218 treatment at a dose of 10^9 cfu/kg per day intragastrically for 8 wk.

By the end of the study, the stool of each mouse was collected and stored at −70°C until analysis. Before sacrifice, mice were fasted for 12 h and anesthetized with diethyl ether. Blood samples were taken from the inferior vena cava for plasma analysis. Liver tissue and intestinal tissue were removed, rinsed with phosphate buffered saline, weighed, and immediately frozen at −70°C. Serum was obtained by centrifugation of blood at 1500 × g for 10 min and stored at −70°C until further analysis. The experimental design was approved by the Ethics Committee of Dalian Medical University, China (SYXK [Liao] 2016-0001).

Biochemical parameters analyzing

The biochemical parameters, including glucose, TG, total cholesterol, low-density lipoprotein cholesterol, high-density lipoprotein cholesterol, serum UA, and alanine aminotransaminase activity, were analyzed with corresponding detection kits (Nanjing Jiancheng Bioengineering Institute, Jiangsu Sheng, China). The concentration of lipopolysaccharide (LPS), interferon-γ (IFN-γ), ATP, AMP, xanthine oxidase (XOD), interleukin-1β (IL-1β), and inosine and the activity of XOD were determined using commercial enzyme-linked immunosorbent assay kits (Lengton, Shanghai, China).

RNA extraction, complementary DNA synthesis, and quantitative real-time PCR

A total of 50 mg of tissue samples were homogenized in 1 mL Trizol reagent (Invitrogen; Thermo Fisher Scientific, Inc., Waltham, MA, USA). Total RNA was extracted from the tissue samples using Trizol reagent following the manufacturer's protocol. The complementary DNA (cDNA) synthesis reaction was performed three times using the M-MuLV First Strand cDNA Synthesis kit (Sangon Biotech Co., Ltd., Shanghai, China) according to the manufacturer's protocol. For real-time quantitative polymerase chain reaction (qPCR), the primers of XOD and β-actin were shown as follows: XOD (forward: 5′-ATGCGGACCCTGAAACAACA-3′, reverse: 5′-TGTTCTGAAGACGGTCATACTTGGA-3′); β-actin (forward: 5′-TGACAGGATGCAGAAGGAGA-3′, reverse: 5′-GCTGGAAGGTGGACAGTGAG-3′). The primers were synthesized by Sangon Biotech Co. Ltd. (Shanghai, China). The relative mRNA expression was expressed as $\Delta Ct = Ct$ (target genes) − Ct (calibrator). The expression of the β-actin gene was used as a calibrator after verification of its stability undercurrent experimental conditions. The relative messenger RNA (mRNA) expression was calculated as $\Delta\Delta Ct = \Delta Ct$ (test group) − ΔCt (control group) and expressed as fold change ($= 2^{-\Delta\Delta Ct}$).

Denaturing gradient gel electrophoresis profiling and sequence analysis

The meta-genomic DNA was extracted from the frozen fecal content of mice by the QIAamp DNA stool mini kit (Qiagen, Hilden, Germany). A NanoDrop 2000 spectrophotometer was used to measure the purity and concentration of the DNA (Thermo Fisher Scientific). PCR was conducted using universal primers F338+GC clamp and R518 targeting the hypervariable V3 region of the 16S ribosomal RNA (rRNA) gene. The resulting 16S ribosomal DNA (rDNA) amplicons were analyzed using the DCode system (Bio-Rad, Hercules, CA, USA) according to a previous description [26]. The digitized denaturing gradient gel electrophoresis (DGGE) images were analyzed as described before [27]. The Shannon-Wiener index of diversity was used to determine the diversity of taxa present in fecal samples collected from the three groups. To identify some separated and strong bands, bands were excised under ultraviolet transilluminator and sequenced as previously described [26].

16S rDNA sequencing and data analysis

The universal primers (520F, 802R) were used to amplify the V3–V4 region of 16S rDNA from metagenomic DNA in mice feces. Primer sets were modified with Illumina adapter regions for sequencing on the IlluminaGAIIx platform (Illumina, San Diego, CA, USA). The reverse primers were modified with an 8-bp Hamming error correcting barcode to distinguish among samples. The 50 μL PCR mixture contained the following components: 100 ng of DNA template, 5 μL PCR buffer, 1 μL dNTPs, 0.25 μL HotStarTaq Plus DNA Polymerase (Qiagen), and 2.5 pmol of each primer. The PCR program consisted of an initial step at 95°C for 5 min; 30 cycles of 94°C for 45 s, 55°C for 45 s, and 72°C for 60 s; and a final extension at 72°C for 8 min. PCR products were checked by 1.5% (weight/volume) agarose gel electrophoresis in 0.5 mg/mL ethidium bromide and purified with the Qiaquick gel extraction kit (Qiagen). Sequences of 16S rDNA were detected by Illumina HiSeq 2000 platform (reconstructed cDNA sequence: 2 × 250 bp). Ribosomal Database Project Classifier 2.8 was used for taxonomical assignment of all sequences at 50% confidence after the raw sequences were identified by their unique barcodes. Operational taxonomic units (OTUs) present in more than 50% the fecal samples were identified as core OTUs. Partial least squares discriminant analysis of core OTUs was performed using Simca-P Version 12 (Umetrics, Sartorius Stedim, Umeå, Sweden). The heat map was generated with Multi-Experiment Viewer (MeV) software to visualize and cluster the microbial community into different groups. Community diversity was measured by the Shannon-Weiner biodiversity index (Shannon index).The data analysis were subsequently performed on an Illumina HiSeq 2000 platform by Personal Biotechnology Co. Ltd (Shanghai, China) as described previously [28].

qPCR evaluation of the abundance of Lactobacillus brevis *in mice*

The abundance of *Lactobacillus brevis* in fecal contents of mice was quantified using the Thermal Cycler Dice Real TimeSystemII (Takara, Japan). Amplification and detection were carried out in 96-well plates using SYBR Premix DimerEraser (Perfect RealTime, Takara, Japan). Each reaction was done in triplicate in a 25 μL total reaction mixture using 2 μL of appropriate dilutions of the DNA sample and 0.3 mM final qPCR primer concentration. The amplification program used was one cycle of 95°C for 1 min, followed by 50 cycles of 95°C for 5s, 55°C for 30 s, 72°C for 30 s, and dissociation at 95°C for 15 s, 60°C for 30 s, and 95°C for 15 s. For construction of the standard curve, the PCR products were generated using the following PCR primers—s-Lbre-F:ATTTTGTTTGAAAGGTGGCTTCGG, s-Lbre-R: ACCCTTGAACAGTTACTCTCAAAGG—and proper dilutions of genomic DNA of *L. brevis* DM9218 were used as templates. The copy numbers of samples were determined by reading off the standard series with the cycle threshold (Ct) values of the samples. Gene copy numbers were expressed as log10 values per gram wet weight of mice fecal samples.

Whole-genome sequencing of DM9218

The overnight culture of DM9218 in MRS medium was treated with 500 μL of TE buffer (25 mM Tris-HCl, pH 8.0, 10 mM EDTA, pH 8.0, and10 mM NaCl) and 1 mg/mL of proteinase K at 37°C, and the genomic DNA was extracted using

phenol-chloroform and alcohol precipitation. DNA was then visualized on an ethidium bromide–stained 0.7% agarose gel. Bacterial genome sequencing was outsourced to Shanghai Personal Biotechnology Co. Ltd (Shanghai, China) and performed using the Illumina Miseq (Illumina). DNA libraries were prepared using TruSeq DNA LT Sample Prep Kits (Illumina) as recommended. A total of 13.2 billion reads were obtained from the library. Genome assembly was performed with ALLPATHLG (http://www.broadinstitute.org/software/ allpaths-lg/blog/).

Heterologous expression of ORF00084 gene and protein purification

The ORF00084 gene was cloned from *Lactobacillus brevis* DM9218 genome DNA with the following primers: 5′ -CCATGGCTAAACGCAAGATGAT-3′ and 5′-CTCGAGGTTCTCTTTGAACAGGT-3′. The 962 bp PCR product was confirmed through electrophoresis and assembled into the plasmid pET28a through *Ncol* and *Xhol* restriction endonuclease sites. *Escherichia coli* DH5α was used for plasmid construction. The construct pET28a-ORF00084 was introduced into *E. coli* BL21 (DE3) cells via electroporation. The positive clone was confirmed by restriction mapping and then cultured in LB broth containing kanamycin (50 μg/mL) at 37°C overnight. For the induction of expression construct, culture was grown till the absorbance of 0.4 at 600 nm and then isopropyl β-D-thiogalactoside (IPTG) was added with a final concentration 100 mM. After 6 h of incubation at 25°C, cells were harvested and suspended in 50 mM Tris buffer, pH 7.5. The cells were sonicated by 6 × 30 s pulses with amplitude of 75% at 4°C (Labsonic U, Melsungen, Germany), and the intracellular fraction was taken for purification. The expressed His-tagged ORF00084 protein was purified with Ni-NTA-Sepharose column by following the manufacturer's instruction.

High-performance liquid chromatography detection of the inosine-degrading activity

A high-performance liquid chromatography (HPLC) system was used to detect both inosine and guanosine simultaneously [25]. The standard samples of inosine and guanosine were purchased from Sigma-Aldrich (St. Louis, MO, USA). To evaluate the inosine and guanosine assimilating ability, the purified His-tagged ORF00084 protein, the supernatant of BL21 cell lysate before and after induced by IPTG were inoculated with the inosine-guanosine solution and incubated at 37°C for 60 min, with shaking (120 rpm). The standard sample solution was used as the control. After that, the solution was centrifuged at 4000 × g, 4°C for 10 min. Then 270 mL of the supernatant was extracted and 30 mL HClO4 (0.1 mol/L) was added into the supernatant, mixed thoroughly to prevent further degradation. After filtration, 20 mL of the mixture was injected into the HPLC device. The remaining inosine and guanosine contents were determined by the peak area at the retention time points 14 and 10 min, respectively.

Statistical analysis

All data were evaluated as mean ± standard error of the mean ($n = 5$). Statistical analysis of the quantitative multiple group comparisons was performed using one-way analysis of variance (and non-parametric), followed by Tukey's test (compare all pairs of columns); when two groups were compared, the non-parametric t test was performed with the assistance of GraphPad Prism 6 (GraphPad Software, La Jolla, CA, USA). Results were considered to be statistically significant with $P < 0.05$.

Results

Effect of DM9218 treatment on metabolic parameters of high-fructose–fed mice

Animal experiments were conducted as shown in Figure 1A. After 8 weeks, as expected, the HF group had an obvious increase in body weight and serum glucose as a result of the high fructose intake compared with the control group (Fig. 1B and C). In addition, serum triglyceride and total cholesterol levels were also increased by the high-fructose diet. Administration of DM9218 had no obvious effect on these events induced by high fructose (Fig. 1D and E). Although some experimental results have found that a high-fructose diet may increase the serum level of low-density lipoprotein cholesterol and decrease the level of high-density lipoprotein cholesterol [29,30], we did not identify any significant change in these two parameters in either the HF group or the probiotic group compared with the control group (Fig. 1F and G). However, it was interesting that the serum uric acid levels, which were remarkably increased in the HF group (both $P < 0.01$ compared with the control group), were reduced by 20% ($P < 0.01$) in the probiotic group compared with the HF group (Fig. 1H). And because in normal mice uric acid is degraded to allantoin by hepatic uricase, which is a defect in humans [31], we also found that the allantoin level was efficiently reduced after treatment of DM9218 (Fig. 1I). Collectively, these findings indicated that DM9218 treatment could efficiently reduce an HF-induced increase of UA and exert some beneficial influence on other metabolic parameters.

Effect of DM9218 on fructose metabolism and UA synthetic pathway in the liver

A synthetic pathway for UA on activation by fructose (based on previous literature) is shown in Fig. 2A. In the liver, fructose is rapidly phosphorylated into fructose-1-phophate in hepatocytes by ketohexokinase, which uses ATP as the phosphate donor, resulting in a reduced level of ATP and intracellular phosphate. Low levels of ATP and intracellular phosphate stimulate the activity of adenosine monophosphate deaminase, which can convert AMP into inosine monophosphate (IMP). Subsequently, IMP is metabolized into inosine by 5'-nucleotidase and further degraded into xanthine by purine nucleoside phosphorylase. Finally, xanthine is converted into hypoxanthine, ultimately generating uric acid via XOD [32]. Some cytokines, such as IFN-γ and IL-1β, are known to up-regulate XOD activity and/or mRNA expression [33–35], which is highly correlated with the bacterial LPS-induced liver inflammation in mice.

To determine whether DM9218 could affect fructose metabolism, we first examined the concentrations of ATP and AMP in the liver. Consistent with previous reports that fructose degradation can consume ATP and increase AMP levels [36], we found that ATP was decreased ($P < 0.01$) and AMP was increased dramatically ($P < 0.001$) in livers of mice in the HF and probiotic-treated groups compared with the control group (Fig. 2B and C). The ratio of AMP to ATP was increased remarkably ($P < 0.001$) (Fig. S1). However, DM9218 treatment had no obvious effect on either the amounts or the ratio of AMP to ATP compared with those in the HF group.

Considering that inosine is an intermediate product during fructose metabolism and may circulate between the liver and gut, we speculated that the ability of DM9218 to degrade inosine in the gut may contribute to the decrease of inosine circulating into the liver; we found previously that DM9218 is an efficient degrader of inosine and guanosine [25]. We therefore monitored the inosine concentration in both the liver and intestinal dejecta. Indeed, the inosine concentration, which was significantly increased ($P < 0.01$) in mice of HF group after fructose consumption, decreased dramatically ($P < 0.01$) after DM9218 treatment in both the liver and excrement of mice in the probiotic group (Fig. 2D and E).

Effect of DM9218 on LPS-induced upregulation of UA synthesis in the liver

Next we wanted to find out whether DM9218 treatment could also affect the hepatic XOD activity. Interestingly, the concentration, mRNA level, and activity of XOD were all markedly increased ($P < 0.001$, $P < 0.01$, $P < 0.01$, respectively, compared with the control group) by high-fructose feeding, but distinctly decreased ($P < 0.05$, $P < 0.001$, $P < 0.05$, respectively, compared with the HF group) by DM9218 treatment (Fig. 2F–H). These findings strongly indicated that DM9218 could retard fructose-induced elevation of XOD activity. It is reported that LPS can induce enterocyte barrier injury and the LPS level in the circulatory system is inversely related to gastrointestinal barrier function [37]. Here we found that high-fructose treatment could significantly ($P < 0.001$) increase the LPS level in the liver, which suggested that high fructose could lead to intestinal dysbiosis and disruption of the intestinal barrier. Previous studies have reported that probiotics can modify the structure of the

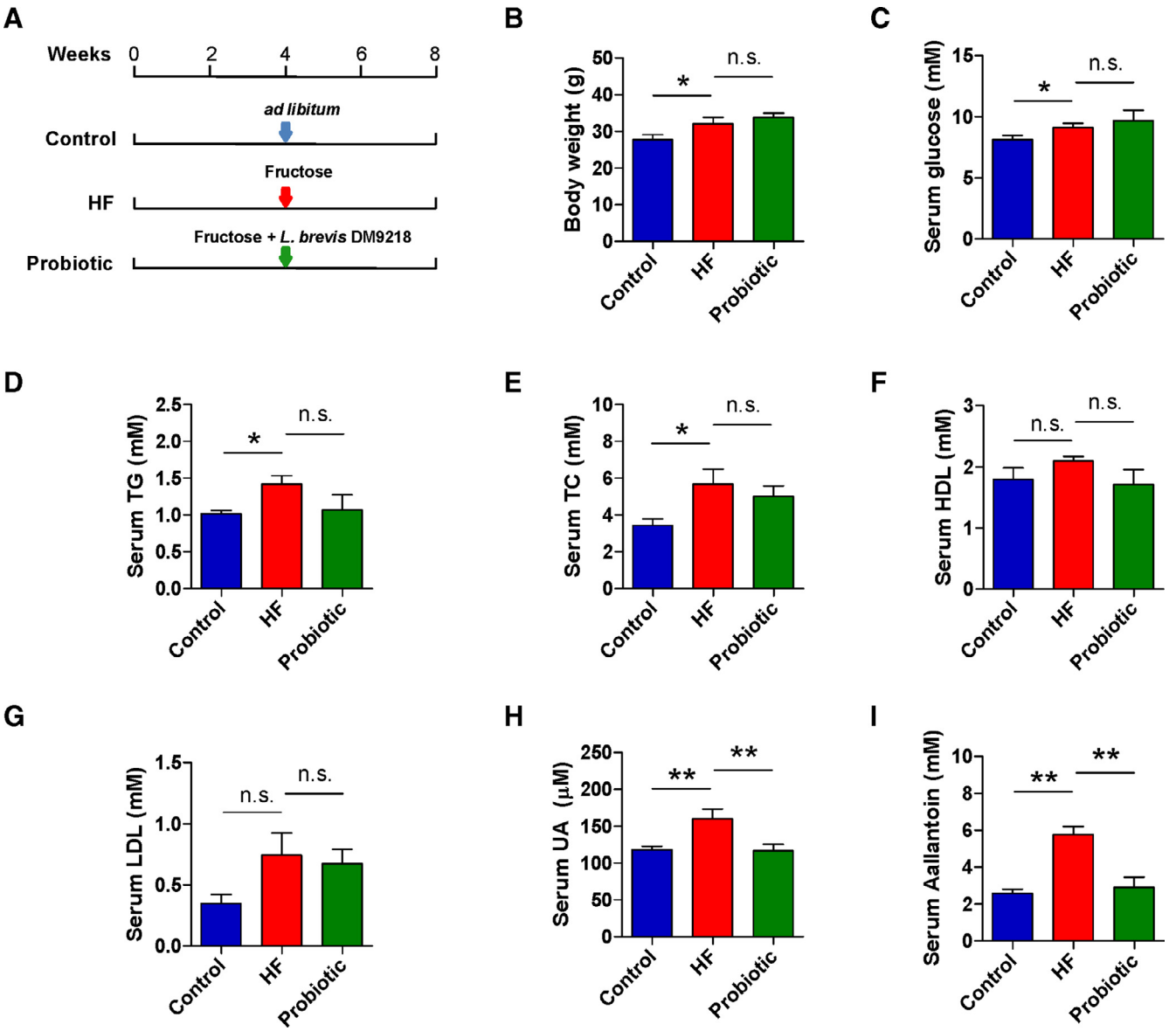

Fig. 1. Effect of DM9218 treatment on metabolic parameters of high-fructose–fed mice. (A) Study design. BALB/c male mice were assigned to three groups ($n = 15$ in each group): a control group fed with standard diet and normal drinking water; a high-fructose group (HF group) with standard diet and 15% fructose solution; and a probiotic-treated group with standard diet, 15% fructose solution, and DM9218 treatment at a dose of 109 cfu/kg per day intragastrically for 8 wk. (B) Body weight of mice, (C) serum glucose, (D) serum triglycerides (TG), (E) serum total cholesterol (TC), (F) serum high-density lipoprotein cholesterol (HDL-C), (G) serum low-density lipoprotein cholesterol (LDL-C), (H) serum uric acid (UA), and (I) allantoin in mice of different groups were detected. Results are expressed as mean ± standard error of the mean ($n = 5$). * $P < 0.05$; ** $P < 0.01$; *** $P < 0.001$. n.s., Nonsignificant.

gut microbiota and improve gastrointestinal barrier function [38]. Like the previous studies, our experimental results indicated that the liver LPS concentration increased by the high-fructose diet was significantly decreased by DM9218 treatment ($P < 0.05$) (Fig. 2I). Notably, the levels of the XOD activity–upregulating cytokines IFN-γ and IL-1β were also remarkably lower in the probiotic group (all $P < 0.01$ compared with the HF group; Fig. 2J, K). Therefore we concluded that DM9218 can improve gastrointestinal barrier function and decrease the level of intestinal proinflammatory cytokines that are increased by a high-fructose diet.

Intestinal microbial composition of high-fructose–fed mice was modified by DM9218

We next investigated the effects of DM9218 on the gut microbiota of high-fructose–treated mice by PCR-DGGE (Fig. 3A). The DGGE fingerprint indicated that the complexity of the microbiota in the HF group differed significantly ($P < 0.001$) from that in the control group (Fig. 3B); the mean number of bands was 36.3 ± 1.53 in the HF group and 44.0 ± 3.29 in the control group. The mean number of bands in the probiotic-treated group was 42.7 ± 3.06, which was much closer to that in the control group and significantly higher ($P < 0.001$) than that in the HF group. Figure 3C shows that there were two main clusters in the dendrogram based on analysis of the DGGE profile: lanes 4, 5, 6 from the HF group and 7, 8, 9 from the probiotic-treated group joined in one cluster, whereas lanes 1, 2, 3 from the control group formed the other cluster. Twelve bands in Figure 3A that were obviously different among the three groups were selected and excised for sequencing analysis. Using the NCBI BLAST sequence analysis tool, the PCR products were found to be similar to sequences of different species listed in Table 1. The gene sequences of DGGE bands 1, 10, 11, and 12 were

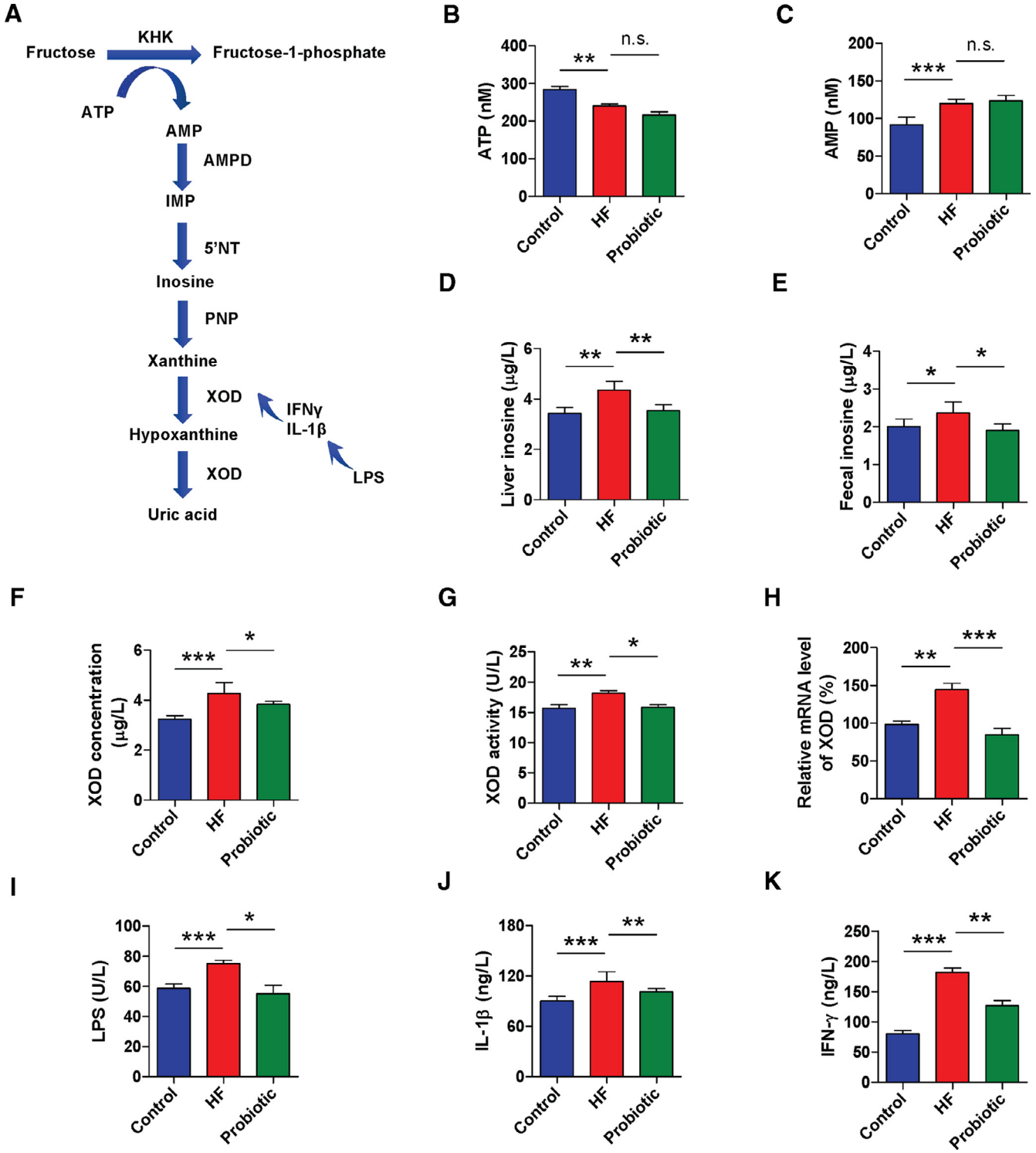

Fig 2. Effect of DM9218 treatment on fructose metabolism and uric acid (UA) synthetic pathway in mice. (A) Synthetic pathway of UA on activation by fructose. (B) The concentration of liver adenosine triphosphate (ATP). (C) The concentration of liver adenosine monophosphate (AMP). (D) The concentration of liver inosine. (E) The concentration of intestinal inosine. (F) The concentration of serum xanthine oxidase (XOD). (G) Serum XOD activity. (H) Relative XOD messenger RNA (mRNA) expression in liver. The concentration of liver lipopolysaccharide (LPS) (I), interleukin-1β (IL-1β) (J), and interferon-γ (IFN-γ) (K) were detected in mice of different groups. Results are expressed as mean ± standard error of the mean ($n = 5$). * $P < 0.05$; ** $P < 0.01$; *** $P < 0.001$. AMPD, adenosine monophosphate deaminase; HF, high-fructose group; IMP, inosine monophosphate; KHK, ketohexokinase, PNP, purine nucleoside phosphorylase; 5′NT, 5′-nucleotidase.

clustered with the gene sequence of *Bacteroides fluxus* YIT 12057, each with an identity of 94%. Bands 2 to 7 were respectively identified as similar to *Clostridium saccharolyticum* strain An168, *Anaerostipes caccae* DSM 14662, *Barnesiella intestinihominis* YIT 11860, *Oceanobacillus picturae* strain S1, *Eubacterium cellulosolvens* 6 and *Marvinbryantia formatexigens* DSM 14469. Bands 8 and 9 showed 95% and 94% similarity to members of the genus *Enterococcus* (*E. casseliflavus* EC20 and *E. thailandicus* strain F0711D, respectively).

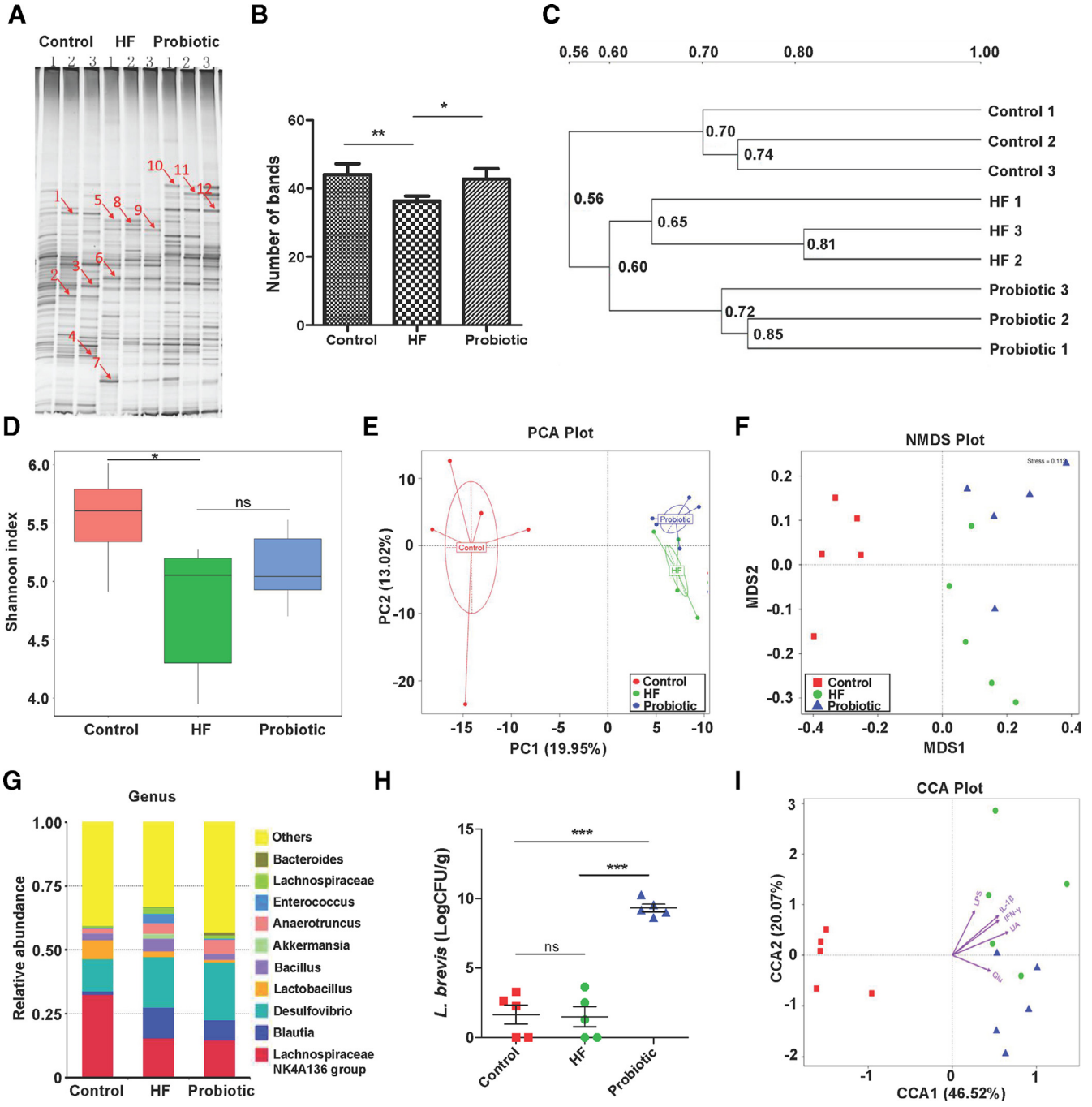

Fig. 3. DM9218 modulated the intestinal dysbiosis in high-fructose–fed mice. (A) DGGE profiles of the V3 region of the 16S rRNA gene amplicons derived from fecal DNA of mice in each group. Bands 1-12 were cut for sequencing. (B) Number of bands. (C) Cluster analysis of the DGGE profiles. The dendrogram was constructed using the UPGMA method. (D) Comparison of the Shannon index of different groups. (E) The principal coordinate analysis (PCA) based on weighted Unifrac distances among different samples. PC1 and PC2 account for 32.97% of the variation. (F) The non-metric multidimensional scaling analysis (NMDS) among different fecal samples. (G) The composition of bacterial composition in different experimental groups at genus level. (H) qPCR detection of the abundance of *Lactobacillus brevis* in fecal samples of mice. (I) The canonical correspondence analysis (CCA) establishes the relationship between the environmental factors and the bacterial community in mice. The direction of arrows indicates correlation with the first two canonical axes and the length of arrows represents the strength of the correlations. Results are expressed as mean ± standard error of the mean ($n = 5$). * $P < 0.05$, ** $P < 0.01$; *** $P < 0.001$. DGGE, denaturing gradient gel electrophoresis; Glu: serum glucose; HF, high-fructose group; IFN-α, interferon-α; IL-1β, interleukin-1β; LPS, lipopolysaccharide; qPCR, quantitative real-time polymerase chain reaction; rRNA, ribosomal RNA; UA, uric acid; UPGMA, *****.

We further adopted metagenomic analysis to systematically characterize the composition of the intestinal microbiota in mouse intestine after DM9218 treatment. There were significant differences between all groups when compared pairwise (Fig. 3D), with the most significant difference observed between the control and HF groups. DM9218 treatment resulted in obvious modification of the bacterial structure of the mouse intestine, as confirmed by principal coordinate analysis (Fig. 3E) and non-metric multidimensional scaling analysis (Fig. 3F). A significant decrease in the abundance of *Bacteroidetes* (phylum) and an elevated abundance of *Verrucomicrobia* (phylum), *Enterococcus* (genus), *Akkermansia* (genus), and *Bacillus* (genus) was detected in HF-treated mice (Fig. 3G and

Table 1
Sequence analysis of 16S rRNA gene fragments identified by PCR-DGGE

Band	Genus name	NCBI accession no.	Identity
1	*Bacteroides fluxus* YIT 12057	NZ_GL882626.1	94%
2	*Clostridium saccharolyticum* strain An168	NZ_NFKU01000053.1	98%
3	*Anaerostipes caccae* DSM 14662	NZ_DS499725.1	95%
4	*Barnesiella intestinihominis* YIT 11860	NZ_JH815206.1	94%
5	*Oceanobacillus picturae* strain S1	NZ_CCAX010000003.1	95%
6	*Eubacterium cellulosolvens* 6	NZ_CM001487.1	95%
7	*Marvinbryantia formatexigens* DSM 14469	NZ_ACCL02000018.1	94%
8	*Enterococcus casseliflavus* EC20	NC_020995.1	95%
9	*Enterococcus thailandicus* strain F0711D	NZ_LWMN01000007.1	94%
10	*Bacteroides fluxus* YIT 12057	NZ_GL882626.1	94%
11	*Bacteroides fluxus* YIT 12057	NZ_GL882626.1	94%
12	*Bacteroides fluxus* YIT 12057	NZ_GL882626.1	94%

PCR-DGGE, polymerase chain reaction–denaturing gradient gel electrophoresis; rRNA, ribosomal RNA.

Fig. S2). Intriguingly, DM9218 treatment resulted in the correction of these bacterial groups to those seen in control mice. However, we did not find an elevation in abundance of total *Lactobacillus* spp. in DM9218-treated group. The bacterial abundance on species level of the 16S rDNA sequencing results indicated that there are mainly *Lactobacillus animalis* and *L. intestinalis* detected in control mice (Fig. S3). After administration of DM9218, the abundance of *L. brevis* increased dramatically in mice intestine; in contrast, the abundance of *L. animalis* and *L. intestinalis* decreased obviously compared with the control mice. Given that the 16S rDNA sequencing method cannot give a quantitative evaluation on bacterial species level, we therefore performed qPCR analysis using primers to specifically detect the abundance of *L. brevis* in mice fecal samples. Our result indicated that the abundance of *L. brevis* in mice treated by DM9218 is markedly higher than that of the control and HF groups (Fig. 3H). Moreover, a canonical correspondence analysis (CCA) was used to establish the relationship between environmental factors (including the UA level, serum glucose, LPS, IFN-α, and IL-1β) and the bacterial community. As shown in Figure 3I, the samples were clearly separated into three groups and the CCA result explained 46.52% and 20.07% of the variation in the first two axes, respectively. The UA, serum glucose, LPS, IFN-α, and IL-1β levels were all closely correlated to the HF group, which was in accordance with our experimental results that high fructose can up-regulate serum glucose and UA levels and weaken intestinal barrier function by increasing LPS, IFN-α, and IL-1β levels. In conclusion, these results indicated that DM9218 can modify the gut microbiota (which was disturbed by high fructose) and improve gastrointestinal barrier function.

An inosine hydrolase gene in Lactobacillus brevis *DM9218 genome was detected*

To delineate the mechanism of inosine decrease induced by DM9218 treatment, next-generation whole-genome sequencing was performed. A total of 5 282 508 reads were obtained, leading to 1 321 776 569 bp of sequence data. The size of the DM9218 genome is 2 535 529 bp, comprising one circular chromosome with 45.74% G+C content. The total number of ORFs is 2485 (2 138 910 bp). The genome contains three rRNAs, 54 tRNAs and 46 ncRNAs. No CRISPRs were detected. The sequencing data for this project has been deposited in DDBJ/ENA/GenBank with accession number QAJZ00000000. The version described in this paper is QAJZ01000000. A graphical circular map of the *L. brevis* DM9218 genome is presented in Figure 4A, and the general features of the genome are listed in Table 2. Functional annotation was performed using KEGG orthology, and a summary of functional categories is shown in Figure 4B. Through BLAST analysis, we found that the DM9218 genome was very similar to the genome of *L. brevis* ATCC 367 (NC_008497.1) (Fig. S5), and therefore we renamed the strain used in the present work from *Lactobacillus plantarum* DM9218 to *Lactobacillus brevis* DM9218. Importantly, we discovered a gene named ORF00084 in the DM9218 genome was 99% identical to the inosine-uridine nucleoside N-ribohydrolase gene of *L. brevis* ATCC 367 through alignment by the National Center for Biotechnology Information BLAST (Basic Local Alignment Search Tool). Results indicated that this protein is highly conserved among *L. brevis* strains (99%) and has high similarities with other *Lactobacillus* strains ranging from 68% to approximately 89% (Fig. S4A), but it is quite different from other organisms such as *E. coli*. (Fig. S4B) (https://blast.ncbi.nlm.nih.gov/smartblast/smartBlast.cgi). We hypothesize that the product of ORF00084 may contribute to the inosine-degrading ability of strain DM9218.

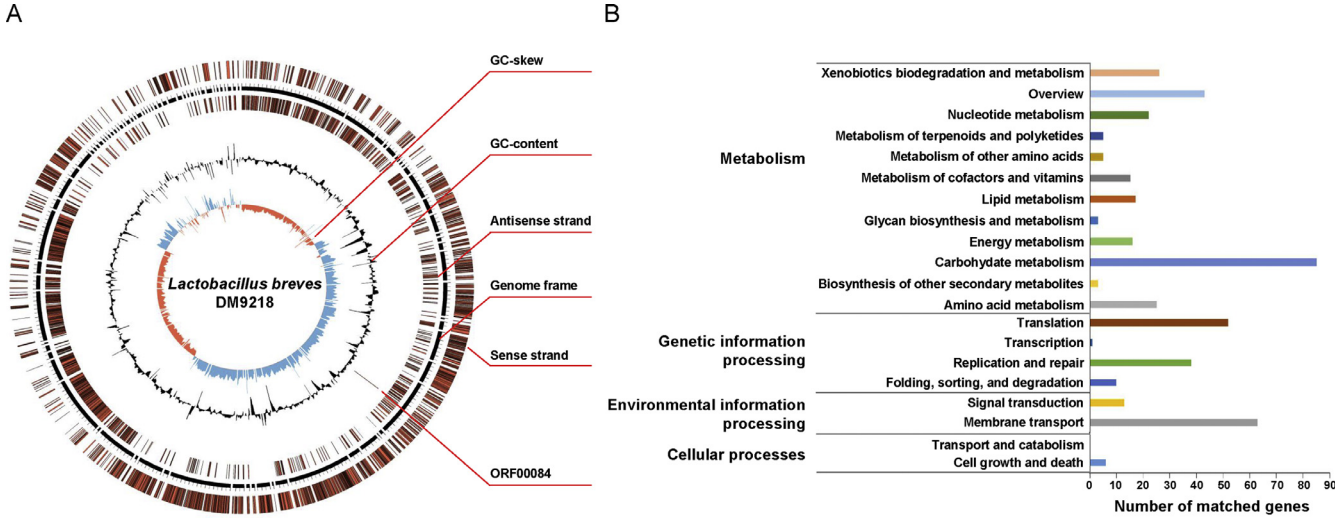

Fig. 4. Whole-genome sequencing of DM9218. (A) The graphical circular map of the *Lactobacillus brevis* DM9218 genome. Circle range is from 1 (inner) to 6 (outer). Circle 1, GC-skew; circle 2, GC-content; circle 3, inosine hydrolase gene ORF00084; circle 4, antisense strand; circle 5, genome frame; circle 6, sense strand. (B) The KEGG orthology (KO) annotation and the summary of functional categories for the predicted genes of *L. brevis* DM9218.

Table 2
General features of *Lactobacillus brevis* DM9218 genome

Property	Contig	Scaffold
Min sequence length	496	2618
Max sequence length	260 831	2 331 362
Total sequence number	92	10
N20	148 148	2 331 362
N20 Number	3	1
N50	83 631	2 331 362
N50 Number	9	1
N90	15 077	2 331 362
N90 Number	35	1
N Number	0	113 934
N rate	0	0.4%
Total sequence length	2 535 529	23 535 529
GC content	45.74%	45.74%
Sequence greater than 1kb	89	10

Max, maximum; Min, minimum; N Number, uncertain base number; N rate, rate of the uncertain base number out of the total base number; N20/50/90, the length of the last sequence when the sum of the sequence length from the longest to the shortest is greater than 20%/50%/90% of the total sequence length; N20/50/90 Number, the sequence number when the sum of the sequence length from the longest to the shortest is greater than 20%/50%/90% of the total sequence length.

Characterization of the inosine hydrolase gene of DM9218

To verify the inosine hydrolyzing ability of *ORF00084*, we cloned it from the strain DM9218 genome into the prokaryotic expression vector pET28a. Recombinant protein was expressed in *E. coli* BL21, purified, and assayed for inosine hydrolysis. SDS-PAGE (sodium dodecyl sulfate polyacrylamide gel electrophoresis) of the purified recombinant protein is shown in Figure 5A. The molecular weight of the protein was about 35 kDa and the purity of the His-tagged protein reached 90% after elution from the nickel-affinity chromatography column with 100 mM imidazole (Fig. 5A). Next we performed HPLC detection to test the enzymatic activity; the concentration of inosine and guanosine (as a control) was determined before and after incubation with the recombinant *E. coli* BL21 or the purified recombinant protein. Before IPTG induction, the *E. coli* could not degrade either guanosine or inosine, whereas after IPTG induction it could assimilate inosine and transform it into other products. After incubation with purified His-tagged ORF00084 protein, there was rarely any inosine detectable in the reaction mixture (Fig. 5B). The inosine degradation rates of both the *E. coli* strain after IPTG induction and the purified His-tagged ORF00084 were significantly higher than those of the controls and uninduced *E. coli* (Fig. 5C). These findings strongly indicate that the ORF00084 gene product was an inosine hydrolase.

Discussion

Fructose, a natural monosaccharide found in many fruits and honeys, is sweeter than glucose and sucrose in equal amounts. An increase in high-fructose corn syrup consumption has been linked with a rise in metabolic disorders in recent decades, which raises concerns regarding the long-term effects of fructose consumption on human health [37,39]. One of the main metabolites of fructose intake is uric acid, which may result in hyperuricemia [40]. Hyperuricemia is not only the main cause of gout but also a risk factor for arteriosclerosis, cardiovascular diseases, and nephropathy in diabetic patients [41]. Therefore, normalizing serum uric acid level is essential to reduce the risk of hyperuricemia and related complications. In the absence of an efficient drug list for asymptomatic hyperuricemia, probiotic treatment is a promising strategy to prevent such diseases. In this study we revealed that DM9218, a probiotic *Lactobacillus brevis* strain isolated from Chinese sauerkraut, can modulate high-fructose–induced intestinal dysbiosis and decrease high-fructose–induced increase of uric acid. Most importantly, we found that the underlying mechanism of this activity is attributable to an inosine hydrolase gene and the manipulation of fructose-induced dysbiosis.

Intriguingly, a dramatic decrease in the level of serum uric acid was identified when mice were fed a high-fructose diet together with DM9218 at a dose of 10^9 cfu/kg per day (intragastrically) compared with the HF group of mice. Uric acid is the ultimate product of fructose metabolism in the liver. Unlike the metabolites and regulatory mechanism of glucose, fructose is metabolized in liver by fructokinase (ketohexokinase), which phosphorylates fructose into fructose-1-phosphate using ATP. Unlike hexokinases, which phosphorylate glucose and have a feedback regulatory mechanism to prevent excessive phosphorylation, fructokinase catalyzes its substrate as fast as it can, resulting in intracellular phosphate depletion. The lower phosphate levels in the cell activate AMP deaminase, transform AMP into IMP, and increase the concentration of inosine, which will finally be degraded into uric acid by XOD. Consistent with previous studies, we found a dramatic decrease of ATP and increase of AMP after high fructose consumption. In addition, the inosine in the liver and the intestine was also increased, as was the XOD concentration, mRNA level, and activity. However, after DM9218 treatment, the levels of all these parameters were modulated to normal. Moreover, the endotoxin LPS and the intestinal proinflammatory cytokine IL-1β, which were increased by the high-fructose diet, were both reduced by DM9218 treatment. It was reported that LPS and IL-1β could up-regulate the XOD mRNA level and activity [34,42]. Thus the decrease of LPS may be the reason for the normalization of XOD activity after DM9218 treatment. LPS is an active endotoxin component, and gut-derived bacterial LPS is brought to the liver by portal circulation [43]. It can induce enterocyte barrier injury and is inversely related to gastrointestinal barrier function [36]. Therefore we supposed that DM9218 may have the ability to modify the intestinal microbiota and strengthen intestinal barrier function.

Of note, it has been reported that high-fructose and high-fat diets may induce intestinal dysbiosis [44]. Probiotics are considered a promising weapon to combat microbial dysbiosis. Through PCR-DGGE and metagenomic analyses, we found that DM9218 treatment resulted in obvious modification of the bacterial structure of the mouse intestine at both the phylum and genus levels. The bacterial composition in the gut has emerged as an important factor in obesity and its related metabolic diseases. Previous research in which a high-fructose diet was given to C57BL/6J mice [45] found a decreased abundance of *Bacteroidetes* and increased abundance of *Proteobacteria* and *Verrucomicrobia*. These results are highly consist with our findings. We also observed a drastic decrease of *Bacteroidetes* in HF-fed mice. Actually, a reduction of *Bacteroidetes* was found in obese patients compared with that of the lean people [46,47]; therefore DM9218 obviously has the potential to increase the *Bacteroidetes* abundance in mice. However, treatment of DM9218 did not identify a reduction effect on the abundance of *Proteobacteria*, which was also found increased in HF-diet mice in a study by Tain et al. [48]. Some studies found that the prior exposure to gastric acids can promote the growth of *Proteobacteria*, resulting in production of metabolites that can improve β-pancreatic cell function and insulin secretion [49]. Thus the role of *Proteobacteria* in high-fructose–induced metabolism syndrome remain unclear. Moreover, we found an elevation in the abundance of *Verrucomicrobia* (phylum) in the gut of HF-treated mice, and this was mainly contributed by the increase of the *Akkermansia*. This genus was found to be associated with a reduction in the protective inner mucus layer, ultimately reducing the intestinal

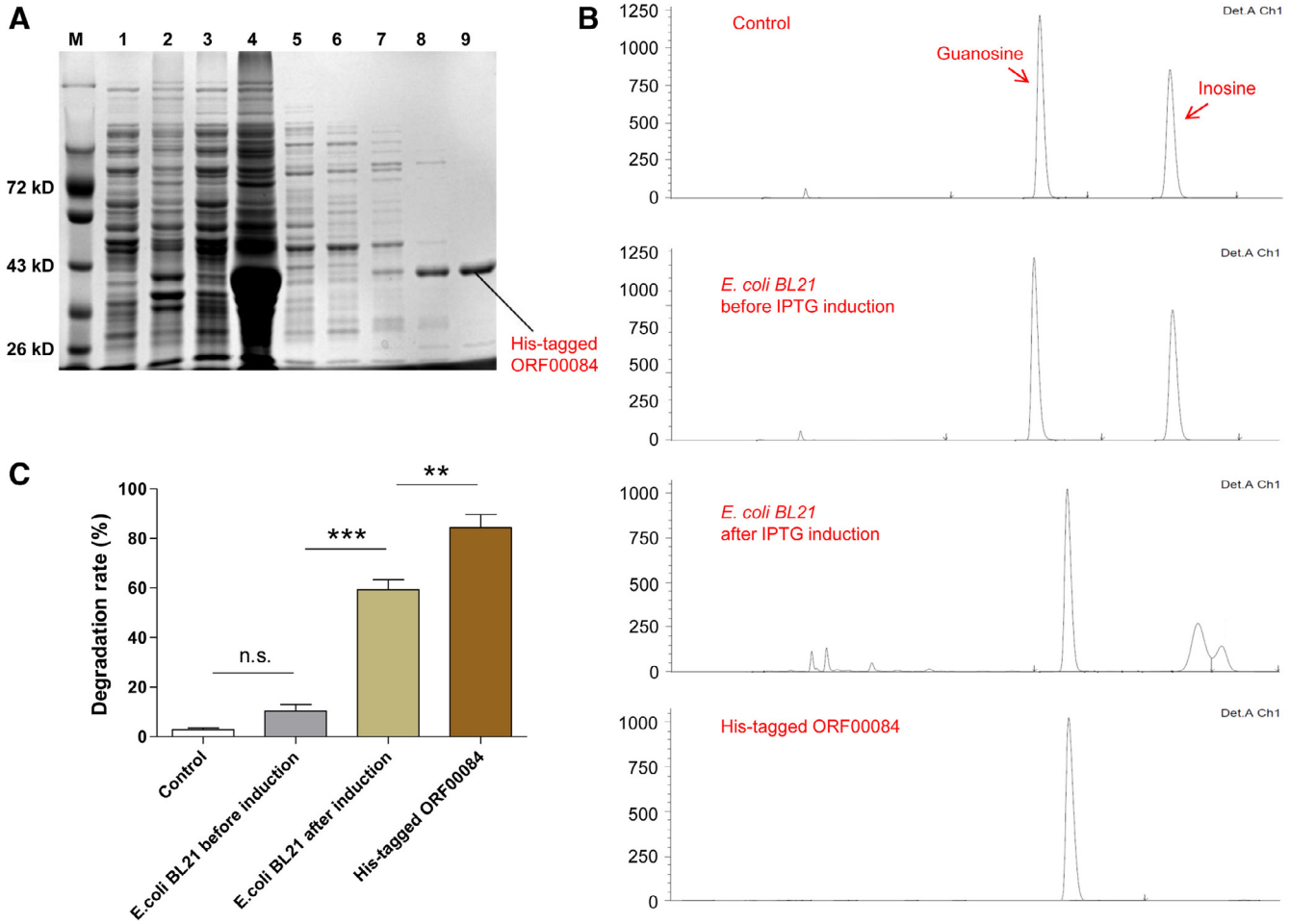

Fig. 5. Heterologous expression and characterization of the inosine hydrolase gene ORF00084. (A) Purification of the His-tagged ORF00084 protein. Protein marker (M); the supernatant (1) and precipitation (2) of BL21 (pET28a-ORF00084) fermentation liquid before isopropyl β-D-thiogalactoside (IPTG) induction; the supernatant (3) and precipitation (4) of BL21 (pET28a-ORF00084) fermentation liquid after IPTG induction; purified ORF00084 protein elucidated by 20 mM imidazole (5), 40 mM imidazole (6), 60 mM imidazole (7), 80 mM imidazole (8), and 100 mM imidazole (9). (B) The degradation of inosine by *Escherichia coli* or purified ORF00084 protein. Control: Inosine and guanosine solution without inoculation of bacteria (270 mL of the inosine and guanosine solution was incubated at 37°C for 60 min; after that 30 mL HClO4 was added, and 20 mL of the mixture was analyzed by HPLC). *E.coli* BL21 before IPTG induction: BL21 living cells before IPTG induction were incubated with inosine and guanosine solution for 60 min. *E.coli* BL21 after IPTG induction: BL21 living cells after IPTG induction were incubated with inosine and guanosine solution for 60 min. His-tagged ORF00084: The purified His-tagged ORF00084 protein was incubated with inosine and guanosine solution for 60 min. (C) The inosine degradation rate of the four groups derived from HPLC analysis. Results are expressed as mean ± standard error of the mean ($n = 5$). * $P < 0.05$; ** $P < 0.01$; *** $P < 0.001$.

barrier integrity and promoting bacterial component and endotoxin leakage from the gastrointestinal tract into the liver [50]. In view of the study by Tain et al. [48] and a previous study reporting an increased abundance of *A. muciniphila* on ingestion of a high-fat high-sucrose diet [51], *Akkermansia* seems to play a negative role in high-fructose–induced metabolism syndromes. Although some other studies in diet-induced obese mice reported that an increase in *Akkermansia spp.* is beneficial for improving glucose homeostasis [52,53], and *Akkermansia muciniphila* was found to negatively affect IFN-γ on glucose metabolism [54], results from our study further highlighted the novel role of *Akkermansia* in high-fructose–induced metabolic syndromes, and administration of DM9218 is obviously effective in maintaining a proper abundance of this genus. In addition, through CCA analysis, we revealed that environmental factors, including UA, serum glucose, LPS, IFN-α, and IL-1β, were closely related to the bacterial community in the HF group. In fact, numerous studies have reported that probiotics can restore gut microbiota, inhibit proliferation of harmful bacteria, improve gastrointestinal barrier function, and delay the progress of liver injury [21,55].

However, the manipulation of intestinal dysbiosis may not be the only way that DM9218 can ameliorate fructose-induced hyperuricemia. Studies have found that some *Lactobacillus* spp., such as *L. panis,* can ferment fructose via the Embden-Meyerhof (EM) pathway [56], and species of *L. kunkeei* and *L. brevis* have been identified as fructophilic *Lactobacillus* [57,58]. In contrast, *L. animalis* spp. was found to be a poor fructose utilizer [59]. Thus there is a possibility that the administrated DM9218 has consumed a large amount of fructose, which results in extra fructose reaching to liver. In addition, based on our previous study [25], DM9128 has the high ability to degrade inosine, which is an intermediate product of fructose metabolism that causes the elevation of serum uric acid. Through whole-genome sequencing and BLAST analysis, we discovered an inosine hydrolase gene (ORF00084) in the genome of strain DM9218. On heterologous expression of the protein in *E. coli* BL21, we found that the BL21 strain gained the ability to assimilate inosine. Purified recombinant ORF00084 protein had high inosine-degradation activity. Increasing the inosine degradation rate in the intestine can reduce the amount of inosine circulating between gut and liver. Therefore, in addition to fructose

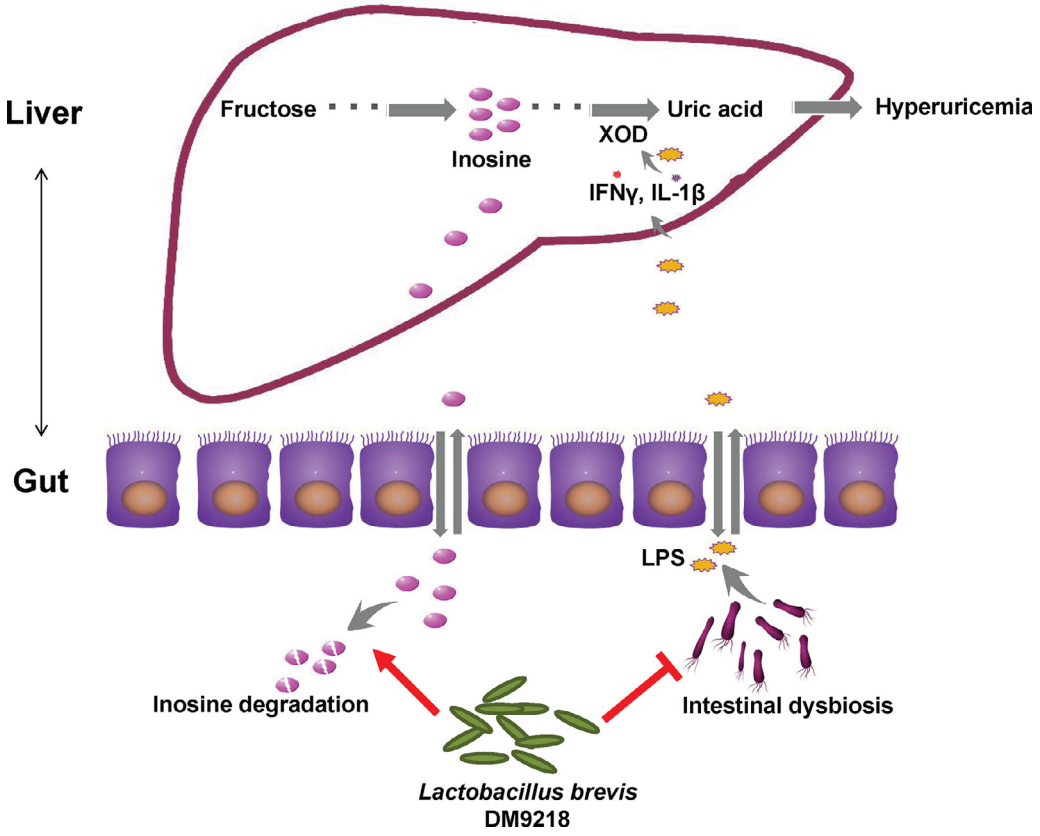

Fig. 6. *Lactobacillus brevis* DM9218 ameliorates fructose-induced hyperuricemia through inosine degradation and manipulation of intestinal dysbiosis. IFNγ, interferon-γ; IL-1β, interleukin-1β; LPS, lipopolysaccharide; XOD, xanthine oxidase.

fermentation, the inosine degradation ability of DM9218 makes it superior to other probiotics regarding the reduction of serum UA levels and thus possess a potential application prospect for the prevention of hyperuricemia.

Conclusions

Lactobacillus brevis DM9218 is a potential probiotic strain that can decrease high-fructose diet–induced uric acid production by degrading the intermediate metabolite inosine in the intestine and thus reduce the circulating amount of inosine in the liver (Fig. 6). DM9218 also has the ability to enhance gastrointestinal barrier function by modifying high-fructose–induced intestinal dysbiosis. In sum, probiotic strain DM9218 shows promise for preventing high-fructose–induced hyperuricemia.

Supplementary materials

Supplementary material associated with this article can be found in the online version at doi:10.1016/j.nut.2018.11.018.

References

[1] Havel PJ. Dietary fructose: implications for dysregulation of energy homeostasis and lipid/carbohydrate metabolism. Nutr Rev 2005;63:133–57.
[2] Zhang DM, Jiao RQ, Kong LD. High dietary fructose: direct or indirect dangerous factors disturbing tissue and organ functions. Nutrients 2017;9:335.
[3] Panasevich MR, Meers GM, Linden MA, Booth FW, Perfield JW, Fritsche KL, et al. High-fat, high-fructose, high-cholesterol feeding causes severe NASH and cecal microbiota dysbiosis in juvenile Ossabaw swine. Am J Physiol Endocrinol Metab 2018;314:E78–92.
[4] Stanhope KL, Medici V, Bremer AA, Lee V, Lam HD, Nunez MV, et al. A dose-response study of consuming high-fructose corn syrup-sweetened beverages on lipid/lipoprotein risk factors for cardiovascular disease in young adults. Am J Clin Nutr 2015;101:1144–54.
[5] Malik VS, Popkin BM, Bray GA, Després JP, Willett WC, Hu FB. Sugar-sweetened beverages and risk of metabolic syndrome and type 2 diabetes. Diabetes Care 2010;33:2477–83.
[6] Dornas WC, de Lima WG, Pedrosa ML, Silva ME. Health implications of high-fructose intake and current research. Adv Nutr 2015;6:729–37.
[7] Brosh S, Boer P, Sperling O. Effects of fructose on synthesis and degradation of purine nucleotides in isolated rat hepatocytes. Biochim Biophys Acta 1982;717:459–64.
[8] Kaneko C, Ogura J, Sasaki S, Okamoto K, Kobayashi M, Kuwayama K, et al. Fructose suppresses uric acid excretion to the intestinal lumen as a result of the induction of oxidative stress by NADPH oxidase activation. Biochim Biophys Acta 2017;1861:559–66.
[9] Sánchez-Lozada LG. The pathophysiology of uric acid on renal diseases. Contrib Nephrol 2018;192:17–24.
[10] Cheng D, Du R, Wu XY, Lin L, Peng K, Ma LN, et al. Serum uric acid is associated with the predicted risk of prevalent cardiovascular disease in a community-dwelling population without diabetes. Biomed Environ Sci 2018;31:106–14.
[11] Choi BG, Kim DJ, Baek MJ, Ryu YG, Kim SW, Lee MW, et al. Hyperuricaemia and development of type 2 diabetes mellitus in Asian population. Clin Exp Pharmacol Physiol 2018;45:499–506.
[12] Kanbay M, Ozkara A, Selcoki Y, Isik B, Turgut F, Bavbek N, et al. Effect of treatment of hyperuricemia with allopurinol on blood pressure, creatinine clearance, and proteinuria in patients with normal renal functions. Int Urol Nephrol 2007;39:1227–33.
[13] Siu YP, Leung KT, Tong MKH, Kwan TH. Use of allopurinol in slowing the progression of renal disease through its ability to lower serum uric acid level. Am J Kidney Dis 2006;47:51–9.
[14] Gois PHF, Souza ERM. Pharmacotherapy for hyperuricemia in hypertensive patients. Cochrane Database Syst Rev 2017;4:CD008652.
[15] Shekelle PG, Newberry SJ, FitzGerald JD, Motala A, O'Hanlon CE, Tariq A, et al. Management of gout: a systematic review in support of an American college of physicians clinical practice guideline. Ann Intern Med 2017;166:37–51.
[16] Freis ED, Sappington R. Long-term effect of probenecid on diuretic-induced hyperuricemia. JAMA 1966;198:127–9.

[17] Choi HK, Liu S, Curhan G. Intake of purine-rich foods, protein, and dairy products and relationship to serum levels of uric acid: the third national health and nutrition examination survey. Arthritis Rheum 2005;52:283–9.
[18] Schmidt JA, Crowe FL, Appleby PN, Key TJ, Travis RC. Serum uric acid concentrations in meat eaters, fish eaters, vegetarians and vegans: a cross-sectional analysis in the epic-oxford cohort. PLoS One 2013;8:e56339. R. P.
[19] Power SE, O'toole PW, Stanton C, Ross G, Fitzgerald F. Intestinal microbiota, diet and health. Br J Nutr 2014;111:387–402.
[20] Guo Z, Zhang J, Wang Z, Ang KY, Huang S, Hou Q, et al. Intestinal microbiota distinguish gout patients from healthy humans. Sci Rep 2016;6:20602.
[21] Gareau MG, Sherman PM, Walker WA. Probiotics and the gut microbiota in intestinal health and disease. Nat. Rev. Gastroenterol Hepatol 2010;7:503–14.
[22] Park DY, Ahn YT, Huh CS, Mcgregor RA, Choi MS. Dual probiotic strains suppress high fructose-induced metabolic syndrome. World J Gastroenterol 2013;19:274–83.
[23] Gerritsen J, Smidt H, Rijkers GT, De Vos WM. Intestinal microbiota in human health and disease: The impact of probiotics. Genes Nutr 2011;6:209–40.
[24] Kajander K, Myllyluoma E, Rajilić-Stojanović M, Kyrnpalo S, Rasmussen M, Jrvenp S, et al. Clinical trial: multispecies probiotic supplementation alleviates the symptoms of irritable bowel syndrome and stabilizes intestinal microbiota. Aliment Pharmacol Ther 2008;27:48–57.
[25] Li M, Yang D, Mei L, Yuan L, Xie A, Yuan J. Screening and characterization of purine nucleoside degrading lactic acid bacteria isolated from Chinese sauerkraut and evaluation of the serum uric acid lowering effect in hyperuricemic rats. PLoS One 2014;9:e105577.
[26] Joossens M, Huys G, Cnockaert M, De Preter V, Verbeke K, Rutgeerts P, et al. Dysbiosis of the faecal microbiota in patients with Crohn's disease and their unaffected relatives. Gut 2011;60:631–7.
[27] Gafan GP, Lucas VS, Roberts GJ, Petrie A, Wilson M, Spratt DA. Statistical analyses of complex denaturing gradient gel electrophoresis profiles. J Clin Microbiol 2005;43:3971–8.
[28] Boon N, De Windt W, Verstraete W, Top EM. Evaluation of nested PCR-DGGE (denaturing gradient gel electrophoresis) with group-specific 16s RRNA primers for the analysis of bacterial communities from different wastewater treatment plants. FEMS Microbiol Ecol 2002;39:101–12.
[29] Yadav H, Jain S, Sinha PR. Antidiabetic effect of probiotic dahi containing lactobacillus acidophilus and lactobacillus casei in high fructose fed rats. Nutrition 2007;23:62–8.
[30] Stanhope KL, Bremer AA, Medici V, Nakajima K, Ito Y, Nakano T, et al. Consumption of fructose and high fructose corn syrup increase postprandial triglycerides, LDL-cholesterol, and apolipoprotein-b in young men and women. J Clin Endocrinol Metab 2011;96:E1596–E605.
[31] Liu Y, Goldfarb DS, El-Achkar TM, Lieske JC, Wu XR. Tamm-Horsfall protein/uromodulin deficiency elicits tubular compensatory responses leading to hypertension and hyperuricemia. Am J Physiol Renal Physiol 2018;314:F1062–F76.
[32] Madlala HP, Maarman GJ, Ojuka E. Uric acid and transforming growth factor in fructose-induced production of reactive oxygen species in skeletal muscle. Nutr Rev 2016;74:259–66.
[33] Dupont GP, Hueckstead TP, Marshall BC, Ryan US, Michael JR, Hoidal JR. Regulation of xanthine dehydrogenase and xanthine oxidase activity and gene expression in cultured rat pulmonary artery endothelial cells. J Clin Invest 1992;89:197–202.
[34] Terao M, Cazzaniga G, Ghezzi G, Bianchi M, Falciani F, Perani P, et al. Molecular cloning of a cDNA coding for mouse liver xanthine dehydrogenase: regulation of its transcript by interferons in vivo. Biochem J 1992;281:863–70.
[35] Kurosaki M, Li M, Calzi E, Scanziani E, Garattini E, Terao M. Tissue- and cell-specific expression of mouse xanthine oxidoreductase gene in vivo: regulation by bacterial lipopolysaccharide. Biochem J 1995;306:225–34.
[36] Vilà L, Roglans N, Perna V, Sánchez RM, Vázquez-Carrera M, Alegret M, Laguna JC. Liver AMP/ATP ratio and fructokinase expression are related to gender differences in AMPK activity and glucose intolerance in rats ingesting liquid fructose. J Nutr Biochem 2011;22:741–51.
[37] Johnson RJ, Segal MS, Sautin Y, Nakagawa T, Feig DI, Kang DH, et al. Potential role of sugar (fructose) in the epidemic of hypertension, obesity and the metabolic syndrome, diabetes, kidney disease, and cardiovascular disease. Am J Clin Nutr 2007;86:899–906.
[38] Xue L, He J, Gao N, Lu X, Li M, Wu X, et al. Probiotics may delay the progression of nonalcoholic fatty liver disease by restoring the gut microbiota structure and improving intestinal endotoxemia. Sci Rep 2017;7:45176.
[39] Lanaspa MA, Tapia E, Soto V, Sautin Y, Sánchez-Lozada LG. Uric acid and fructose: Potential biological mechanisms. Semin Nephrol 2011;31:426–32.
[40] Jamnik J, Rehman S, Blanco Mejia S, de Souza RJ, Khan TA, Leiter LA, et al. Fructose intake and risk of gout and hyperuricemia: a systematic review and meta-analysis of prospective cohort studies. BMJ Open 2016;6:e013191.
[41] Johnson RJ, Perez-Pozo SE, Sautin YY, Manitius J, Sanchez-Lozada LG, Feig DI, et al. Hypothesis: could excessive fructose intake and uric acid cause type 2 diabetes? Endocr Rev 2009;30:96–116.
[42] Hassoun PM, Yu FS, Cote CG, Zulueta JJ, Sawhney R, Skinner KA, et al. Upregulation of xanthine oxidase by lipopolysaccharide, interleukin-1, and hypoxia. Am J Respir Crit Care Med 1998;158:299–305.
[43] Chen Y, Wu Z, Yuan B, Dong Y, Zhang L, Zeng Z. MicroRNA-146a-5p attenuates irradiation-induced and LPS-induced hepatic stellate cell activation and hepatocyte apoptosis through inhibition of TLR4 pathway. Cell Death Dis 2018;9:22.
[44] Rosas-Villegas A, Sánchez-Tapia M, Avila-Nava A, Ramírez V, Tovar A, Torres N. Differential effect of sucrose and fructose in combination with a high fat diet on intestinal microbiota and kidney oxidative stress. Nutrients 2017;9:393.
[45] Do M, Lee E, Oh M-J, Kim Y, Park H-Y. High-glucose or -fructose diet cause changes of the gut microbiota and metabolic disorders in mice without body weight change. Nutrients 2018;10:761.
[46] Riva A, Borgo F, Lassandro C, Verduci E, Morace G, Borghi E, et al. Pediatric obesity is associated with an altered gut microbiota and discordant shifts in firmicutes populations. Environ Microbiol 2017;19:95–105.
[47] Turnbaugh PJ, Ley RE, Mahowald MA, Magrini V, Mardis ER, Gordon JI. An obesity-associated gut microbiome with increased capacity for energy harvest. Nature 2006;444:1027.
[48] Tain Y-L, Lee W-C, Wu K-L-H, Leu S, Chan J-Y-H. *Resveratrol prevents the development of hypertension programmed by maternal plus post-weaning high-fructose consumption through modulation of oxidative stress, nutrient-sensing signals, and gut microbiota. Mol Nutr Food Res 2018;62:1800066.
[49] Cani PD, Delzenne NM. The role of the gut microbiota in energy metabolism and metabolic disease. Curr Pharm Des 2009;15:1546–58.
[50] Yılmaz Yusuf FE. Future perspectives on probiotics in metabolic liver diseases. Turk J Gastroenterol 2017;28:327–8.
[51] Carmody RN, Gerber GK, Luevano JM, Gatti DM, Somes L, Svenson KL, et al. Cell Host Microbe 2015;17:72–84.
[52] Shin NR, Lee JC, Lee HY, Kim MS, Whon TW, Lee MS, et al. An increase in the *Akkermansia* spp. population induced by metformin treatment improves glucose homeostasis in diet-induced obese mice. Gut 2014;63:727–35.
[53] Anhê FF, Roy D, Pilon G, Dudonné S, Matamoros S, Varin TV, et al. A polyphenol-rich cranberry extract protects from diet-induced obesity, insulin resistance and intestinal inflammation in association with increased *Akkermansia* spp. population in the gut microbiota of mice. Gut 2015;64:872–83.
[54] Greer RL, Dong X, Moraes ACF, Zielke RA, Fernandes GR, Peremyslova E, et al. *Akkermansia muciniphila* mediates negative effects of IFNγ on glucose metabolism. Nat Commun 2016;7:13329.
[55] Wang Y, Liu Y, Sidhu A, Ma Z, McClain C, Feng W. Lactobacillus rhamnosus GG culture supernatant ameliorates acute alcohol-induced intestinal permeability and liver injury. Am J Physiol Gastrointest Liver Physiol 2012;303:G32–41.
[56] Kang TS, Korber DR, Tanaka T. Regulation of dual glycolytic pathways for fructose metabolism in heterofermentative *Lactobacillus panis* PM1. Appl Environ Microbiol 2013;79:7818–26.
[57] Neveling DP1, Endo A, Dicks LM. Fructophilic *Lactobacillus kunkeei* and *Lactobacillus brevis* isolated from fresh flowers, bees and bee-hives. Curr Microbiol 2012;65:507–15.
[58] Gustaw K, Michalak M, Polak-Berecka M, Waśko A. Isolation and characterization of a new fructophilic *Lactobacillus plantarum* FPL strain from honeydew. Ann Microbiol 2018;68:459–70.
[59] Lua Y, Putraa SD, Liua SQ. A novel non-dairy beverage from durian pulp fermented with selected probiotics and yeast. Int J Food Microbiol 2018;265:1–8.